Divisor Dynamics for Surface Fluid Simulation

RUDRESH VEERKHARE, HANG YIN, and ALBERT CHERN, University of California San Diego, USA

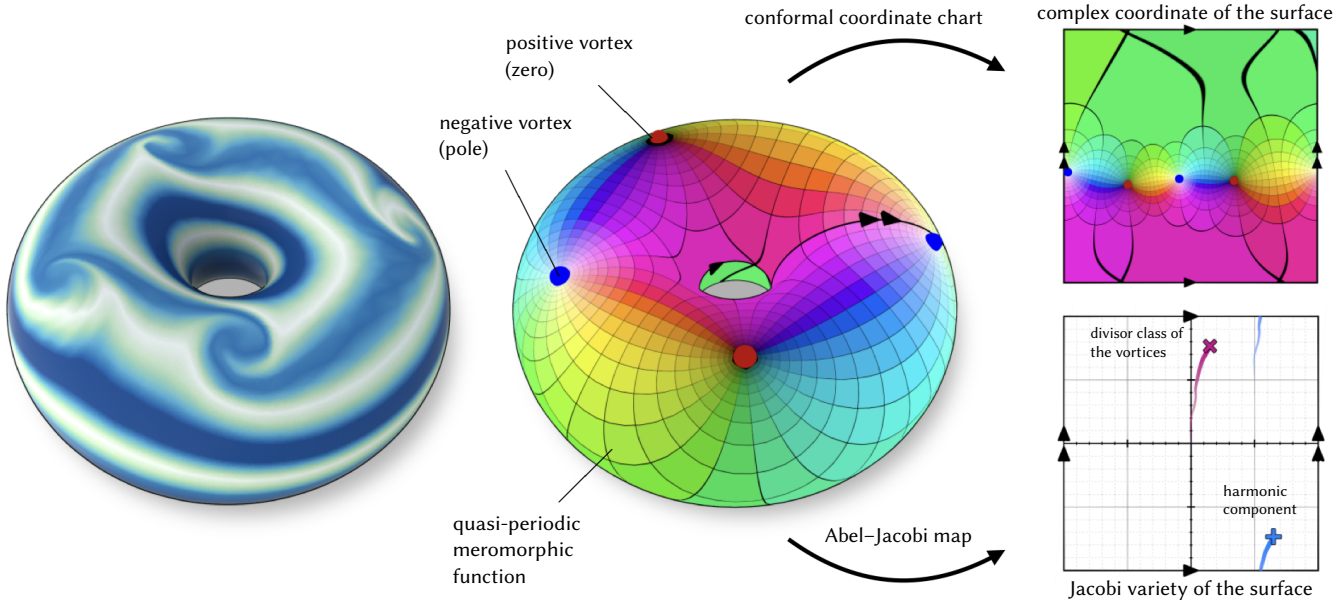


Fig. 1. A point-vortex method for fluid simulation on surfaces with arbitrary topology (left). The point-vortex configuration defines a *divisor* on a Riemann surface (middle and top-right), corresponding to the zeros and poles of a quasi-periodic meromorphic function whose logarithmic magnitude encodes the streamfunction. The *Abel–Jacobi map* evaluates the divisor class in the *Jacobi variety* (bottom-right). We show that the difference between the harmonic component and the Abel–Jacobi image of the vortex divisor is a conserved quantity. Exploiting this invariant, we obtain a point-vortex solver that naturally incorporates the harmonic component.

We introduce a simulation method for point vortices on surfaces with arbitrary topology. We show that incorporating the dynamics of the harmonic components on a non-simply-connected surface is equivalent to introducing a new fluid invariant that is conserved over time. This invariant admits an elegant formulation in terms of the divisor class of point vortices, viewed as a divisor on a Riemann surface. To clarify this connection, we establish a nontrivial bridge between fluid dynamics and the theory of divisors in algebraic geometry. By exploiting this invariant, our simulation method becomes a simple modification of the vortex particle-on-mesh method, which extends its applicability to surfaces with arbitrary topology.

CCS Concepts: • **Computing methodologies** → **Physical simulation**; • **Mathematics of computing** → **Algebraic topology**; *Differential equations.*

Additional Key Words and Phrases: Point vortex; Abel–Jacobi map.

ACM Reference Format:
Rudresh Veerkhare, Hang Yin, and Albert Chern. 2026. Divisor Dynamics for Surface Fluid Simulation. In *SIGGRAPH Asia 2026 Conference Papers (SA Conference Papers '26), December 01–04, 2026, Kuala Lumpur, Malaysia.* ACM, New York, NY, USA, 10 pages. https://doi.org/10.1145/3829340.3842224

Authors' Contact Information: Rudresh Veerkhare, rveerkhare@ucsd.edu; Hang Yin, h7yin@ucsd.edu; Albert Chern, alchern@ucsd.edu, University of California San Diego, La Jolla, CA, USA.

This work is licensed under a Creative Commons Attribution 4.0 International License.
SA Conference Papers '26, Kuala Lumpur, Malaysia
© 2026 Copyright held by the owner/author(s).
ACM ISBN 979-8-4007-2842-6/2026/12
https://doi.org/10.1145/3829340.3842224

1 Introduction

Simulating incompressible fluids on curved surfaces is a central problem in computer graphics [Yaeger et al. 1986; Stam 2003; Shi and Yu 2004] and computational fluid dynamics [Nitschke et al. 2017]. In recent years, simulation methods have advanced significantly through the combination of vorticity formulations and geometry processing techniques [Azencot et al. 2014; Cui et al. 2021; Yin et al. 2023; Tao et al. 2024; Zhu et al. 2025]. In this paper, we study a reduced model for two-dimensional incompressible Euler equations: the *point vortex model*. When the vorticity is concentrated into Dirac δ-distributions, it remains so for all time. This reduces the fluid equations to a finite-dimensional dynamical system governing the motion of a finite collection of point vortices.[1]

The flow associated with a point-vortex configuration is well understood in the planar case through potential theory and complex analysis [Batchelor 1967, § 6.5]. Since the vorticity is zero almost everywhere, the flow is potential except for isolated singularities at the vortex locations. The configuration can be described directly using a *meromorphic function* whose *zeros* and *poles* represent positive

[1]Note its difference from *vortex particle methods* [Selle et al. 2005] which supply additional eddies to a fluid solver. Here, the entire fluid state is described by a finite set of point vortices.

and negative vortices. Because of this relationship, complex-analytic techniques have long been standard tools for producing exact flow solutions in two-dimensional [Joukowsky 1910; Saffman 1992, Ch. 7; Aref 2007; Crowdy et al. 2016]. In addition to their conceptual elegance, point-vortex models are numerically advantageous: vorticity is represented by Lagrangian particles, which avoids the numerical dissipation and dispersion that typically arise when vorticity is discretized as Eulerian fields under advection. Owing to these features, point-vortex formulations and their numerical methods have become classic exercises in the simulation of planar fluids.

Although extensions of point-vortex theory to the sphere have been known for some time [Bogomolov 1977; Vankerschaver and Leok 2014], major developments for general curved surfaces emerged only much more recently [Boatto and Koiller 2008]. Boatto and Koiller showed that the effective interaction energy for point vortices (the *Kirchhoff–Routh function*) includes an additional *Robin function* term. Padilla [2018] developed a numerical method for point-vortex simulation on surfaces that incorporates the Robin function through the conformal scaling factor associated with the conformal map from the surface to the sphere. More recently, Tao et al. [2024] introduced a vortex particle-on-mesh method that retains point vortices as Lagrangian particles while computing the streamfunction on an Eulerian mesh with classical geometry processing tools, thereby bypassing the need to evaluate the Robin function explicitly.

However, the above theories and methods are restricted to simply-connected surfaces. On higher-genus surfaces, the interaction between the vorticity and the harmonic component of the velocity field cannot be neglected [Nitschke et al. 2021]. This interaction was analyzed and computed explicitly in [Yin et al. 2023; Zhu et al. 2025] for smooth vorticity fields. For point vortices, the corresponding harmonic interaction term in the Kirchhoff–Routh function was derived in [Grotta-Ragazzo et al. 2024]. So far, there is no numerical point-vortex method on surfaces with arbitrary topology.

In this paper, we present the first point-vortex solver for surfaces with arbitrary topology. We discover that the point-vortex dynamics on high-genus surfaces admits an additional invariant, which can be expressed as a function of both the vortex positions and the harmonic component. This conservation law is previously pointed out by Yin et al. [2023], but only in terms of the notion of relative linking numbers rather than an explicit function of the vorticity configuration. The existence of this invariant enables a reduction of the dynamical system by expressing the harmonic component directly in terms of the vortex positions and the value of the invariant. Remarkably, this invariant is encoded by the *divisor class* of the vortices, viewed as a *divisor* on a compact Riemann surface. This perspective leads to a simple numerical method when combined with the vortex particle-on-mesh scheme [Tao et al. 2024], and reveals a new connection between fluid dynamics and algebraic geometry.

Our solver offers several practical advantages over existing methods. Unlike [Tao et al. 2024], our method incorporates the correct harmonic component. Compared with the function-based vorticity representation of [Yin et al. 2023], point vortices are less susceptible to numerical dissipation and dispersion, making our method better suited for sharply concentrated vorticity.

2 Theory

We may assume the fluid domain is a closed surface M without loss of generality. To extend the theory to surfaces with boundary, apply the double cover trick detailed in [Zhu et al. 2025, § 4.1]; that is, duplicate the surface, glue them along the boundary, and keep the proper parity symmetry of each field. See also App. A.

Let $\mathbf{u} \in \Gamma(TM)$ be the velocity field of an inviscid incompressible fluid. Let $\eta \coloneqq \mathbf{u}^\flat$ denote the corresponding velocity covector (1-form). The incompressibility of the fluid velocity translates to that η is coclosed: $d \star \eta = 0$. In general, η is not closed, *i.e.* it has a vorticity field $\omega = d\eta \in \Omega^2(M)$.[2]

A point vortex configuration is a fluid state where the vorticity field is concentrated to isolated points $\mathbf{p}_1, \dots, \mathbf{p}_N \in M$, each of which has a vortex strength κ_i. That is, the vorticity 2-form is

$$\omega = \textstyle\sum_{i=1}^N \kappa_i \delta_{\mathbf{p}_i} \tag{1}$$

where $\delta_{\mathbf{p}}$ denotes the Dirac-δ measure (formally a 2-form, or a 0-current) at point $\mathbf{p}$. The strength corresponds to the circulation $\kappa_i = \oint_{C_i} \eta$ of a small loop C_i enclosing $\mathbf{p}_i$ (and no other point vortices). For ω to be in the image of the exterior derivative $\omega = d\eta$, the strengths necessarily satisfy $\sum_{i=1}^N \kappa_i = 0$.

The dynamics of these point vortices are straightforward: they are advected by the fluid flow, and the strengths κ_i are invariant over time:

$$\tfrac{d}{dt}\mathbf{p}_i = \mathbf{u}|_{\mathbf{p}_i}, \quad \tfrac{d}{dt}\kappa_i = 0, \quad i = 1, \dots, N. \tag{2}$$

Note that the velocity $\mathbf{u}$ is typically singular at each $\mathbf{p}_i$. This singular evaluation $\mathbf{u}|_{\mathbf{p}_i}$ of the velocity is taken as the *Lebesgue point value*, equivalently the mean value in infinitesimal disk:

$$\mathbf{u}|_{\mathbf{p}} \coloneqq \lim_{\epsilon \to 0} \tfrac{1}{|B_\epsilon(\mathbf{p})|} \iint_{B_\epsilon(\mathbf{p})} \mathbf{u}\, dA, \tag{3}$$

where $B_\epsilon(\mathbf{p})$ denotes the geodesic ϵ-disk centered at $\mathbf{p}$. For $\mathbf{u}$ being tangent vectors, the integral viewed as componentwise sum of $\mathbf{u}$ technically depends on the choice of basis field. Nevertheless, on a smooth surface M, after taking the limit, this componentwise evaluation is independent of this choice of basis.

For a simply-connected surface M, equation (2) is a complete autonomous system since the variable $\mathbf{u} = \eta^\sharp$ is uniquely determined by the vorticity $\omega = \sum_{i=1}^N \kappa_N \delta_{\mathbf{p}_i}$, precisely through a Poisson equation

$$\eta = \star d\psi, \quad d \star d\psi = \textstyle\sum_{i=1}^N \kappa_i \delta_{\mathbf{p}_i}, \tag{4}$$

where $\psi \in \Omega^0(M)$ is called the *streamfunction*.

However, on a non-simply-connected domain, (2) is no longer a closed system, as $\mathbf{u}$ is no longer uniquely determined by the vorticity data. On a closed genus g surface M, there is a $2g$-dimensional space $\mathcal{H}^1(M) = \{\zeta \in \Omega^1 \mid d\zeta = 0, d \star \zeta = 0\}$ of harmonic 1-forms, corresponding to divergence-free and curl-free velocity fields. In the presence of harmonic fields, the velocity 1-form takes a more general form than (4) by including a harmonic component

$$\eta = \underbrace{\star d\psi}_{\eta_{\text{stream}}} + \textstyle\sum_{k=1}^{2g} c_k \zeta_k, \quad d \star d\psi = \textstyle\sum_{i=1}^N \kappa_i \delta_{\mathbf{p}_i}, \tag{5}$$

[2] Our theory is written in exterior calculus [Wang et al. 2023]. See also [Elcott et al. 2007; Yin et al. 2023] for an introduction of this language applied to fluids.

where $\zeta_1, \dots, \zeta_{2g}$ is some fixed basis for $\mathcal{H}^1(M)$, and $c_1, \dots, c_{2g}$ is the time-dependent coefficients for the harmonic component. We call the first part $\eta_{\text{stream}} = \star d\psi$ of (5) the *streamfunction velocity*, which is still uniquely determined by the vorticity ω by the Poisson equation $d \star d\psi = \omega$. To close the system (2), one must include the time-evolution equation for the coefficients $c_1, \dots, c_{2g}$. This time-evolution equation for the harmonic component is given by [Yin et al. 2023] and [Grotta-Ragazzo et al. 2024]:

$$\tfrac{d}{dt} c_k = \iint_M (-\iota_{\mathbf{u}} \omega) \wedge \xi_k \quad k = 1, \dots, 2g, \tag{6}$$

where $\iota_{\mathbf{u}}$ denotes the interior product, and $\xi_1, \dots, \xi_{2g} \in \mathcal{H}^1(M)$ is the dual basis to $\zeta_1, \dots, \zeta_{2g}$ satisfying $\int_M \zeta_k \wedge \xi_\ell = \delta_{k\ell}$.

However, the expression $\iota_{\mathbf{u}}\omega$ in (6) is singular when ω consists of δ measures, and the singularity is much worse than that in (2) regularized by (3). At $\mathbf{p}_i$, $\mathbf{u}$ is unbounded and discontinuous, and inserting it into $\kappa_i \delta_{\mathbf{p}_i}$ to compute (6) would make the integral ill-defined.

In order to incorporate (6) stably, we transform the equation to a more robust conservation law. In practice, incorporating the dynamics of the harmonic component amounts to keeping some invariants constant. These invariants are directly related to the notion of *divisor class group* in algebraic geometry, when the point vortices on M are viewed as a *divisor* on a Riemann surface.

2.1 Vortices and Divisors

Here, we establish the bridge between Riemann surface theory and fluid dynamics. The fluid domain M equipped with the Hodge star operator $\star$ applied to 1-forms is known as a *Riemann surface*. Some of the following background on Riemann surfaces can be found in [Forster 2012; Lee 2024], as well as in [Gu and Yau 2008, Ch. 6] from a geometry processing perspective.

2.1.1 Divisors. A **divisor** is a formal combination of distinct points on a compact Riemann surface M

$$D = \textstyle\sum_{i=1}^N \kappa_i [\mathbf{p}_i] \tag{7}$$

where each κ_i is an integer. The brackets around $\mathbf{p}_i$ are to prevent interpreting D as linear combination of the position coordinate vectors. The space of all divisors is denoted by

$$\mathrm{Div}(M) = \left\{ \textstyle\sum_{i=1}^N \kappa_i [\mathbf{p}_i] \,\middle|\, \kappa_i \in \mathbb{Z}, \mathbf{p}_i \neq \mathbf{p}_j \in M; N \in \mathbb{N}_{\geq 0} \right\}. \tag{8}$$

For $\kappa_i \in \mathbb{R}$, (7) is called a real-coefficient divisor (or real divisor). The space of real divisors is denoted by

$$\mathrm{Div}(M; \mathbb{R}) \coloneqq \mathrm{Div}(M) \otimes_{\mathbb{Z}} \mathbb{R}. \tag{9}$$

The space $\mathrm{Div}(M)$ is an Abelian group under formal addition of points, and the space $\mathrm{Div}(M; \mathbb{R})$ is a vector space over $\mathbb{R}$.

The total sum of the coefficients is called the **degree** of a divisor

$$\deg(D) \coloneqq \textstyle\sum_{i=1}^N \kappa_i, \quad \text{for } D = \sum_{i=1}^N \kappa_i [\mathbf{p}_i]. \tag{10}$$

The space of degree zero divisors is denoted by

$$\mathrm{Div}_0(M) = \{D \in \mathrm{Div}(M) \mid \deg(D) = 0\}, \tag{11}$$

$$\mathrm{Div}_0(M; \mathbb{R}) = \{D \in \mathrm{Div}(M; \mathbb{R}) \mid \deg(D) = 0\}. \tag{12}$$

Each point vortex configuration corresponds to an element of $\mathrm{Div}_0(M; \mathbb{R})$. In particular, each divisor is associated with a Dirac-δ measure, denoted by

$$\delta_D \coloneqq \textstyle\sum_{i=1}^N \kappa_i \delta_{\mathbf{p}_i} \quad \text{for } D = \sum_{i=1}^N \kappa_i [\mathbf{p}_i]. \tag{13}$$

2.1.2 Classification of Divisors. In complex analysis, each element of $\mathrm{Div}(M)$ corresponds to a prescribed set of *zeros* and *poles*. Points with positive integer weights κ are zeros, and those with negative integer weights are poles. Such a divisor corresponds to vortices with integer strengths.

If M is a topological sphere, every divisor $D = \sum_{i=1}^N \kappa_i [\mathbf{p}_i] \in \mathrm{Div}_0(M)$ admits a meromorphic function whose zeros and poles match those prescribed by D. This meromorphic function can be written explicitly as

$$f \colon M \to \mathbb{C} \cup \{\infty\}, \quad f = \exp(2\pi(\psi + \mathbb{i}\varphi)), \tag{14}$$

where $\psi \colon M \to \mathbb{R}$ is precisely the streamfunction solving

$$d \star d\psi = \delta_D \tag{15}$$

and the phase $\varphi \colon M \to \mathbb{R}/\mathbb{Z}$ is locally the harmonic conjugate of ψ away from the points in D, satisfying

$$-d\varphi = \star d\psi = \eta_{\text{stream}}. \tag{16}$$

The condition (16) ensures that f is holomorphic away from D:

$$\bar{\partial} f \coloneqq \tfrac{1}{2}(df - \mathbb{i} \star df) = 0 \quad \text{on } M \setminus \{\mathbf{p}_1, \dots, \mathbf{p}_N\}. \tag{17}$$

The potential function φ for $\eta_{\text{stream}} = \star d\psi$ can be obtained by

$$\varphi(\mathbf{p}) = \textstyle\int_{\mathbf{p}_0}^{\mathbf{p}} -\eta_{\text{stream}} \tag{18}$$

for any fixed point $\mathbf{p}_0 \notin \{\mathbf{p}_1, \dots, \mathbf{p}_N\}$. This integral is well-defined modulo $\mathbb{Z}$, since $d\eta_{\text{stream}} = 0$ away from D, and $\oint_\gamma \eta_{\text{stream}}$ along any loop γ enclosing points of D is an integer due to $\kappa_i \in \mathbb{Z}$.

If M has a non-zero genus, the phase reconstruction (18) is no longer path-independent. In general, the circulations of η_{stream} along loops around the handles of the surface are not integer-valued. Consequently, a generic divisor $D \in \mathrm{Div}_0(M)$ on a non-simply-connected surface does not admit a meromorphic function. Instead, it admits only a quasi-periodic meromorphic function (Figure 1) that acquires a phase jump after traversing a nontrivial global cycle. The obstruction to the existence of a global meromorphic function is given by the non-integer global circulations of η_{stream}.

This leads to the following property of the configuration of (integer-strength) point vortices on a high-genus surface.

Definition 2.1. *A divisor $D \in \mathrm{Div}_0(M)$ is a **principal divisor** if it is the zeros and poles of some meromorphic function.*

Definition 2.2. *Two divisors $D_1, D_2 \in \mathrm{Div}(M)$ are **linearly equivalent**, denoted by $D_1 \sim D_2$, if $D_1 - D_2$ is a principal divisor. The equivalence class of divisors is called the **divisor class group**.*

The following *Abel–Jacobi map* provides a quantitative coordinate for the divisor class group.

2.1.3 Abel–Jacobi Map. The compact Riemann surface M has a $2g$-dimensional space of harmonic 1-forms $\mathcal{H}^1(M) = \{\zeta \in \Omega^1(M) \, d\zeta = 0, d \star \zeta = 0\}$. Let us also consider the space of integral 1-form $H^1(M; \mathbb{Z}) = \{\alpha \in \mathcal{H}^1(M) \mid \oint_\gamma \alpha \in \mathbb{Z} \text{ for all closed loop } \gamma\}$, which forms an integer lattice in $\mathcal{H}^1(M)$.

Definition 2.3. *The **Jacobi variety**[3] or **Jacobian** of a Riemann surface M is the $2g$-dimensional torus defined as the quotient of the vector space of harmonic 1-forms by the lattice of integral forms*

$$\mathrm{Jac}(M) \coloneqq \mathcal{H}^1(M)/H^1(M;\mathbb{Z}). \tag{19}$$

Definition 2.4. *The **Abel–Jacobi map**[4] of a Riemann surface M is the map $\mathrm{AJ}_{\mathbf{p}_0} : M \to \mathrm{Jac}(M)$ for an origin $\mathbf{p}_0 \in M$ is defined so that*

$$\iint_M \mathrm{AJ}_{\mathbf{p}_0}(\mathbf{p}) \wedge \xi \coloneqq \int_{\mathbf{p}_0}^{\mathbf{p}} \xi \quad \text{for all } \xi \in (\mathcal{H}^1(M))^* = \mathcal{H}^1(M). \tag{20}$$

The characterization (20) defines $\mathrm{AJ}_{\mathbf{p}_0}(\mathbf{p}_0) \in \mathrm{Jac}(M)$ via its dual pairing with any linear functionals $\int_M (\cdot) \wedge \xi$ on $\mathrm{Jac}(M)$. For different paths connecting $\mathbf{p}_0$ and $\mathbf{p}$, the values of $\int_{\mathbf{p}_0}^{\mathbf{p}} \xi$ differ only by $\oint_\gamma \xi = \iint_M \delta_\gamma \wedge \xi$ for closed loops γ, and loops are integer-valued forms $[\delta_\gamma] \in H^1(M;\mathbb{Z})$. Thus, $\int_{\mathbf{p}_0}^{\mathbf{p}} \xi$ indeed defines an element in $\mathrm{Jac}(M)$.

More explicitly, a basis for $\mathcal{H}^1(M)$ provides a coordinate system for $\mathrm{Jac}(M)$. Let $\zeta_1, \dots, \zeta_{2g} \in \mathcal{H}^1(M)$ be a basis, and let $\xi_1, \dots, \xi_{2g} \in \mathcal{H}^1(M)$ be its dual basis satisfying $\int_M \zeta_k \wedge \xi_\ell = \delta_{k\ell}$. Then the $\mathbb{R}^{2g}$ coordinates of $\mathrm{AJ}_{\mathbf{p}_0}(\mathbf{p}) \in \mathrm{Jac}(M)$ are given by

$$\mathrm{AJ}_{\mathbf{p}_0}(\mathbf{p}) = \textstyle\sum_{k=1}^{2g} a_k(\mathbf{p})\zeta_k, \quad a_k(\mathbf{p}) = \int_{\mathbf{p}_0}^{\mathbf{p}} \xi_k. \tag{21}$$

The coordinate vector $\mathbf{a}$ is defined modulo the integer lattice generated by the periods $\oint_\gamma \xi_k$, where $\gamma \in H_1(M;\mathbb{Z}) \cong \mathbb{Z}^{2g}$.

The definition of Abel–Jacobi map can be extended to divisors.

Definition 2.5. $\mathrm{AJ}(D) \coloneqq \sum_{i=1}^N \kappa_i \mathrm{AJ}_{\mathbf{p}_0}(\mathbf{p}_i)$ *for* $D = \sum_{i=1}^N \kappa_i [\mathbf{p}_i]$.

Proposition 2.1. *The map* $\mathrm{AJ}\colon \mathrm{Div}_0(M) \to \mathrm{Jac}(M)$ *is linear*[5] *and is independent of the choice of* $\mathbf{p}_0$.

Proof. Linearity follows immediately from Definition 2.5. From (21), changing the origin from $\mathbf{p}_0$ to $\mathbf{p}_0'$ shifts the coordinates by $a_k'(\mathbf{p}) - a_k(\mathbf{p}) = \int_{\mathbf{p}_0}^{\mathbf{p}_0'} \xi_k$. When applied to a degree-0 divisor D, the shift becomes $a_k'(D) - a_k(D) = \sum_{i=1}^N \kappa_i (a_k' - a_k) = (\sum_{i=1}^N \kappa_i)(\int_{\mathbf{p}_0}^{\mathbf{p}_0'} \xi_k)$ $= \deg(D)(\int_{\mathbf{p}_0}^{\mathbf{p}_0'} \xi_k) = 0$. □

Proposition 2.2 (Abel–Jacobi Theorem)**.** *A divisor $D \in \mathrm{Div}_0(M)$ is a principal divisor if and only if* $\mathrm{AJ}(D) = 0$ *(*i.e. *the lattice point of* $\mathrm{Jac}(M)$*). In particular,* $\mathrm{AJ}\colon (\mathrm{Div}_0(M)/\sim) \xrightarrow{\cong} \mathrm{Jac}(M)$ *is an isomorphism between the degree-0 divisor class group and the Jacobi variety.*

Proof. The only obstruction for $D \in \mathrm{Div}_0(M)$ being principal is the path dependency in (18) by the non-integer periods $\oint_\gamma \eta_{\text{stream}}$ of the streamfunction velocity. Let $\Gamma = (\gamma_1, \dots, \gamma_{2g})$ be any set of generators of $H_1(M)$ so that $M \setminus \Gamma$ is a simply-connected fundamental domain and γ_k does not intersect D. The coefficients $\mathbf{a}$ of AJ are smooth $\mathbb{R}^{2g}$-valued functions on $M \setminus \Gamma$ with $da_k = \xi_k$, with jumps at Γ denoted by $[a_k]$. One checks that these jumps are constants given by the periods $\oint_{\gamma_\ell} \xi_k$. Now, $a_k(D) = \sum_{i=1}^N \kappa_i a_k(\mathbf{p}_i) = \iint_{M\setminus\Gamma} a_k \delta_D = \iint_{M\setminus\Gamma} a_k d \star d\psi$ and integration by parts yields $= \oint_\Gamma [a_k] \star d\psi - \iint_{M\setminus\Gamma} \xi_k \wedge \star d\psi = \oint_\Gamma [a_k] \eta_{\text{stream}}$ (using that $\langle\!\langle \xi_k, \star d\psi \rangle\!\rangle = 0$) $= \sum_{\ell=1}^{2g} [a_\ell] \oint_{\gamma_\ell} \eta_{\text{stream}}$. Therefore, global periods $\oint_{\gamma_\ell} \eta_{\text{stream}} \in \mathbb{Z}$ if and only if $\mathbf{a}(D)$ lies on the lattice point of $\mathrm{Jac}(M)$. Hence $\ker(\mathrm{AJ})$ is the space of principal divisors. Upon a straightforward verification that $\mathrm{AJ}\colon \mathrm{Div}_0(M) \to \mathrm{Jac}(M)$ is surjective, we have $\mathrm{AJ}\colon (\mathrm{Div}_0(M)/\sim) \to \mathrm{Jac}(M)$ being an isomorphism. □

One can interpret $\mathrm{AJ}(D)$ as a "center of mass" of the vortices D, with the mass being the vortex strengths that can be negative. The coordinate grid for expressing this center of mass is given by the integrals of the dual harmonic basis $\xi_1, \dots, \xi_{2g}$. The natural target space of this center is the Jacobi variety of M. The Abel–Jacobi Theorem yields a nontrivial information about this center of vortices: The potential φ of the potential flow η_{stream} away from the vortices is a globally well-defined phase function if and only if this center of vortices is zero.

2.1.4 Extension to Real Divisors. The above classification of divisors assumes that the weights κ_i are integer. This assumption is needed for the interpretation of D as prescribing zeros and poles. Now, the characterization of the divisor class group via the Abel–Jacobi map allows us to extend this notion to real divisors. In particular, $\mathrm{AJ}\colon \mathrm{Div}_0(M;\mathbb{R}) \to \mathrm{Jac}(M)$ from Definition 2.5 remains well defined by the same argument used in Proposition 2.1.

Definition 2.6. *Two degree-0 real divisors $D_1, D_2 \in \mathrm{Div}_0(M;\mathbb{R})$ are said to belong to the same **divisor class** if* $\mathrm{AJ}(D_1) = \mathrm{AJ}(D_2)$.

This extends the notion of divisor class group to vortices with general (not necessarily integer-valued) strengths.

2.2 Fluid Invariants

In this section, we show that (6) corresponds to the conservation of an invariant that can be evaluated explicitly using the notions established in Section 2.1.

Let $D \in \mathrm{Div}_0(M;\mathbb{R})$ be a time-dependent divisor representing the configuration of point vortices. Let $\eta_{\text{stream}} = \star d\psi$, where $d \star d\psi = \delta_D$. Write the fluid velocity 1-form as $\eta = \eta_{\text{stream}} + h$, where $h \in \mathcal{H}^1(M)$ is the time-dependent harmonic component of the flow.

Let $[h] \in \mathcal{H}^1(M)/H^1(M;\mathbb{Z})$ denote the projection of h onto the Jacobi variety $\mathrm{Jac}(M) = \mathcal{H}^1(M)/H^1(M;\mathbb{Z})$.

With this setup, we obtain our main theorem.

Theorem 2.1. *Under the incompressible Euler flow, the difference*

$$\mathrm{AJ}(D) - [h] \in \mathrm{Jac}(M) \tag{22}$$

between the divisor class of the point vortices and the harmonic component is conserved.

Proof. Fix a basis $\zeta_1, \dots, \zeta_{2g}$ for $\mathcal{H}^1(M)$, and let $\xi_1, \dots, \xi_{2g} \in \mathcal{H}^1(M)$ be the dual basis. Express $h = \sum_{k=1}^{2g} c_k \zeta_k$, where c_k satisfies (6). Note that c_k are the coordinates for $[h] \in \mathrm{Jac}(M)$. Choose a set of generators $\Gamma = (\gamma_1, \dots, \gamma_{2g})$ for $H_1(M;\mathbb{Z})$. As in the proof of Proposition 2.2, the coefficients $a_k\colon M \setminus \Gamma \to \mathbb{R}$ of the Abel–Jacobi

[3] $\mathrm{Jac}(M)$ is a complex g-dimensional torus with $-\star$ being its complex structure. It is equipped with a Hermitian form $\langle\!\langle \zeta, \xi \rangle\!\rangle_{\mathbb{C}} \coloneqq \int_M \zeta \wedge \star\xi - \mathrm{i} \int_M \zeta \wedge \xi$, whose imaginary part $\int_M (\cdot) \wedge (\cdot)$ is integer-valued when restricted to the lattice $H^1(M;\mathbb{Z})$. This integral condition ensures, via the *Kodaira Embedding Theorem*, that the manifold $\mathrm{Jac}(M)$ can be embedded into complex projective space, and is therefore a projective variety.

[4] Classical definitions of the Abel–Jacobi map use a *canonical basis* (the "a- and b-cycles") for $H_1(M)$, which yields a $\mathbb{C}$-linear coordinate system on $\mathrm{Jac}(M)$. Our basis-free definition is equivalent to these classical ones. Avoiding a canonical basis is more convenient for our purposes, as it allows flexibility in choosing a basis for $\mathcal{H}^1(M)$ that need not be dual to the canonical cycles.

[5] Here, "linear" means a homomorphism of abelian groups, since neither the domain nor the codomain is a vector space.

map (21), satisfying $da_k = \xi_k$, are well defined on $M \setminus \Gamma$, with jumps $[a_k]$ that are constant on each component of Γ and determined by the lattice structure of $\mathrm{Jac}(M)$. Now, starting with (6) we calculate

$$\begin{aligned}\frac{d}{dt}c_k &= \iint_M (-\iota_{\mathbf{u}}\omega)\wedge\xi_k = \iint_{M\setminus\Gamma}(-\iota_{\mathbf{u}}\omega)\wedge\xi_k = \iint_{M\setminus\Gamma}(-\iota_{\mathbf{u}}\omega)\wedge da_k \\ &= \oint_\Gamma(\iota_{\mathbf{u}}\omega)[a_k] - \iint_{M\setminus\Gamma}(d\iota_{\mathbf{u}}\omega)a_k. \end{aligned} \tag{23}$$

If the point vortices are not supported on Γ (which can be guaranteed by an appropriate choice of Γ), then the first term in (23) vanishes, and the integration domain $M\setminus\Gamma$ in the second term can be extended to M. By Cartan's formula for the Lie derivative operator $\mathscr{L}_{\mathbf{u}}$ and $d\omega = 0$, we have $d\iota_{\mathbf{u}}\omega = \mathscr{L}_{\mathbf{u}}\,\omega = -\frac{\partial}{\partial t}\omega$ (by the vorticity equation $\frac{\partial}{\partial t}\omega + \mathscr{L}_{\mathbf{u}}\,\omega = 0$). Continuing from (23), we obtain

$$\frac{d}{dt}c_k = \iint_M(\tfrac{\partial}{\partial t}\omega)a_k = \frac{d}{dt}\iint_M \omega a_k = \frac{d}{dt}\iint_M \delta_D a_k = \frac{d}{dt}a_k(D). \tag{24}$$

Removing $\frac{d}{dt}$ from both sides yields that $a_k(D) - c_k$ are constants of motion. These are the coefficients for $\mathrm{AJ}(D) - [h] \in \mathrm{Jac}(M)$. □

Remark 2.1. *The conservation law* (22) *corresponds to the invariance of the difference between the cross-sectional flux c_k and the linking number* $\textsc{Link}(\omega)(\xi_k)$ *between harmonic streamlines and the vortex lines, as discovered in [Yin et al. 2023, Thm. 2]. In particular,* $\textsc{Link}(\omega)(\xi_j) = \iint_M \omega U_j$ *in [Yin et al. 2023, § 3.4.3] on a multi-annulus corresponds to our quantity* $\iint_M \omega a_k$ *in* (24)*. However, for higher-genus domains,* $\textsc{Link}(\omega)(\cdot)$ *is defined only in a relative sense. In examples such as [Yin et al. 2023, § 5.1], where the vorticity is constant, the linking number cannot be a well-defined function of the vorticity alone, since the vorticity is stationary while c_k evolves dynamically.*

The significance of Theorem 2.1 is that, when ω is configured as point vortices, Yin et al. [2023]'s invariant can finally be explicitly evaluated as (22)*, a well-defined function of the positions of the vortices and the magnitudes of the harmonic components. In the context of simulations, that allows us to express the harmonic component as a function of D and the initial value of* $\mathrm{AJ}(D) - [h]$*, and thereby eliminate h from the state variables of the dynamical system.*

In summary, the equations of motion for vortex dynamics on surfaces are as follows. Let $\mathbf{p}_1, \dots, \mathbf{p}_N$ be the position of N vortices with time-independent strengths $\kappa_1, \dots, \kappa_N \in \mathbb{R}$, satisfying $\sum_{i=1}^N \kappa_i = 0$. Let $h_0 \in \mathcal{H}^1(M)$ be an initial harmonic field. Define the constant of motion $C = \mathrm{AJ}(\sum_{i=1}^N \kappa_i[\mathbf{p}_i]) - [h_0] \in \mathrm{Jac}(M)$. Then the evolution of the vortex positions and the harmonic component is governed by

$$\begin{cases} \frac{d\mathbf{p}_i}{dt} = \mathbf{u}|_{\mathbf{p}_i}, \quad i = 1, \dots, N, \\ \mathbf{u} = (\star d\psi + h)^\sharp, \\ d\star d\psi = \sum_{i=1}^N \kappa_i \delta_{\mathbf{p}_i}, \\ \mathrm{AJ}(\sum_{i=1}^N \kappa_i[\mathbf{p}_i]) - [h] = C. \end{cases} \tag{25}$$

3 Discretization

We describe a method for simulating (25) for point vortices on a triangle mesh based on a hybrid of Eulerian and Lagrangian schemes. The setup is similar to the method of vortex particle-on-mesh [Tao et al. 2024]. The point vortices are Lagrangian particles with general positions in the triangles. The streamfunction ψ, harmonic field h, and the final velocity field $\mathbf{u}$ are stored on the mesh, whose evaluations at general positions are interpolated.

3.1 Spatial Discretization

Let $\mathsf{M} = (\mathsf{V}, \mathsf{E}, \mathsf{F})$ be a triangle mesh. The streamfunction $\boldsymbol{\psi}\colon \mathsf{V} \to \mathbb{R}$ is stored on vertices interpolated as a piecewise linear function, and harmonic fields are piecewise constant vector fields. In the following, let $\phi_{\mathsf{v}} \in C^0(M)$, $\mathsf{v} \in \mathsf{V}$, denote the piecewise linear finite element basis (hat functions). That is, ϕ_{v} is globally continuous, affine in each triangle, and equals to 1 at vertex v, and 0 at every other vertex.

3.1.1 Vortex to Streamfunction Solve. In the smooth setting, each vortex configuration $D = \sum_{i=1}^N \kappa_i[\mathbf{p}_i]$ determines a streamfunction ψ via the Poisson solve $d\star d\psi = \delta_D$. In the discrete setting, we first map the point vortex configuration D to a discrete vorticity field $\boldsymbol{\omega}\colon \mathsf{V} \to \mathbb{R}$ followed by a standard discrete Poisson solve as in the Discrete Exterior Calculus and the Functional Fluids framework [Elcott et al. 2007; Azencot et al. 2014; Yin et al. 2023; Tao et al. 2024].

Given each $D = \sum_{i=1}^N \kappa_i[\mathbf{p}_i]$ define $\boldsymbol{\omega}\colon \mathsf{V} \to \mathbb{R}$ by

$$\omega_{\mathsf{v}} \coloneqq \textstyle\sum_{i=1}^N \kappa_i \phi_{\mathsf{v}}(\mathbf{p}_i). \tag{26}$$

Equivalently, $\boldsymbol{\omega}$ is the result of iterating through the vortices $i = 1, \dots, N$, and cumulatively assigning κ_i times the barycentric coordinates of $\mathbf{p}_i$ to the vertices of the triangle that contains $\mathbf{p}_i$.

The divisor-to-vorticity map (26) is mathematically natural in the context of the piecewise linear finite element scheme. Let $\mathcal{I}\colon \mathbb{R}^{\mathsf{V}} \to C^0(M)$ denote the linear map of piecewise-linear interpolation $(\mathcal{I}\mathbf{f})(\mathbf{p}) \coloneqq \sum_{\mathsf{v}\in\mathsf{V}} f_{\mathsf{v}}\phi_{\mathsf{v}}(\mathbf{p})$. Consider the adjoint $\mathcal{I}^*$ of $\mathcal{I}$, which maps the dual space $(C^0(M))^*$ of the space of continuous functions to $\mathbb{R}^{\mathsf{V}*}$. Note that the dual space of continuous function is the space $\mathcal{M}(M)$ of signed measures (that are finite and Borel-regular). In particular, this space of measures contain point measures: $\delta_D \in \mathcal{M}(M) \cong C^0(M)^*$, with dual pairing given by $\langle\delta_D|g\rangle = \iint_M \delta_D g = \sum_{i=1}^N \kappa_i g(\mathbf{p}_i)$ for any $g \in C^0(M)$. Therefore, the canonical adjoint $\mathcal{I}^*$ of $\mathcal{I}$ can be applied to δ_D. Setting $\boldsymbol{\omega} \in \mathbb{R}^{\mathsf{V}}$ as

$$\boldsymbol{\omega} = \mathcal{I}^*\delta_D, \tag{27}$$

then by $\langle\boldsymbol{\omega}|\mathbf{f}\rangle = \langle\delta_D|\mathcal{I}\mathbf{f}\rangle$ for all $\mathbf{f} \in \mathbb{R}^{\mathsf{V}}$, we obtain (26).

After obtaining the discrete vorticity field $\boldsymbol{\omega} \coloneqq \mathcal{I}^*\delta_D \in \mathbb{R}^{\mathsf{V}*}$ we solve for $\boldsymbol{\psi} \in \mathbb{R}^{\mathsf{V}}$ the discrete Poisson equation $-\mathbf{L}\boldsymbol{\psi} = \boldsymbol{\omega}$, where $\mathbf{L}\colon \mathbb{R}^{\mathsf{V}} \to \mathbb{R}^{\mathsf{V}*}$ is the discrete cotangent Laplacian $\mathbf{L} = \mathbf{d}_0^\intercal \star_1 \mathbf{d}_0$ in Discrete Exterior Calculus (DEC) [Hirani 2003; Crane et al. 2013], equivalently the stiffness matrix $(\mathbf{L})_{\mathsf{vw}} = \iint_M \operatorname{grad}\phi_{\mathsf{v}} \cdot \operatorname{grad}\phi_{\mathsf{w}}\, dA$.

Note that the discrete streamfunction $\boldsymbol{\psi} = -\mathbf{L}^{-1}\mathcal{I}^*\delta_D$ from the point vortex divisor D is exactly the Galerkin solution to the Poisson equation $\Delta\psi = \delta_D$. That is, $\iint_M(\Delta(\mathcal{I}\boldsymbol{\psi}) - \delta_D)(\mathcal{I}\mathbf{f})\,dA = 0$ for all piecewise linear test functions $\mathcal{I}\mathbf{f}$.

3.1.2 Evaluating Streamfunction Velocity. The streamfunction $\boldsymbol{\psi} \in \mathbb{R}^{\mathsf{V}}$ constructed via $\boldsymbol{\psi} = -\mathbf{L}^{-1}\mathcal{I}^*\delta_D$ defines a piecewise constant velocity field by

$$\bar{\mathbf{u}}_{\text{stream}} = \mathcal{J}\operatorname{grad}\boldsymbol{\psi} = \mathcal{J}\textstyle\sum_{\mathsf{v}\in\mathsf{V}}\psi_{\mathsf{v}}\operatorname{grad}\phi_{\mathsf{v}} \tag{28}$$

where $\mathcal{J}$ is the facewise 90° rotation operator. However, directly evaluating $\bar{\mathbf{u}}_{\text{stream}}$ at the point vortices $\mathbf{p}_i$ does not capture the result of the singular evaluation (3). For the Lebesgue value (3), the singularity of $\mathbf{u}_{\text{stream}}|_{\mathbf{p}_i}$ is canceled out through the averaging, resulting in a value smoothly dependent on $\mathbf{p}_i$. By contrast, $\bar{\mathbf{u}}_{\text{stream}}|_{\mathbf{p}_i}$ is dominated by the position $\mathbf{p}_i$ within a triangle.

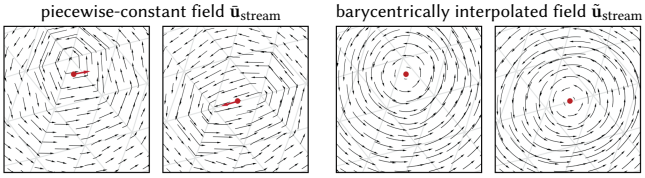


Fig. 2. The discrete streamfunction velocity fields associated with a point vortex, computed directly from the discrete streamfunction (28) ($\bar{\mathbf{u}}_{\text{stream}}$, left) and using the averaging scheme (30) ($\tilde{\mathbf{u}}_{\text{stream}}$, right). The piecewise-constant velocity $\bar{\mathbf{u}}_{\text{stream}}$, when evaluated at the vortex, is sensitive to the vortex location within the triangle, and exhibits discontinuities across edges. In contrast, $\tilde{\mathbf{u}}_{\text{stream}}$ is continuous and varies smoothly with the vortex position.

To remedy the qualitatively incorrect evaluation of $\bar{\mathbf{u}}_{\text{stream}}$, we perform a pre-averaging step to account for the averaging expression (3). This is the velocity interpolation method in [Elcott et al. 2007, § 4.4] and [Tao et al. 2024, § 4.6]. Explicitly, we first represent (28) as $\mathbb{R}^3$-valued vectors $\bar{\mathbf{u}}_{\text{stream}} \colon \mathsf{F} \to \mathbb{R}^3$, tangential to the embedded surface in $\mathbb{R}^3$. Average the facewise velocity to vertices:

$$\hat{\mathbf{u}}_{\text{stream}} \colon \mathsf{V} \to \mathbb{R}^3, \quad \hat{\mathbf{u}}_{\text{stream}}|_{\mathsf{v}} \coloneqq \tfrac{1}{\sum_{\mathsf{f}\succ\mathsf{v}} A_{\mathsf{f}}} \textstyle\sum_{\mathsf{f}\succ\mathsf{v}} \bar{\mathbf{u}}_{\text{stream}}|_{\mathsf{f}} A_{\mathsf{f}} \tag{29}$$

where A_{f} denotes the triangle area. Then define the continuous, piecewise linear velocity field by the barycentric interpolation

$$\tilde{\mathbf{u}}_{\text{stream}} \in C^0(M;\mathbb{R}^3), \quad \tilde{\mathbf{u}}_{\text{stream}} \coloneqq \textstyle\sum_{\mathsf{v}\in\mathsf{V}} \hat{\mathbf{u}}_{\text{stream}} \phi_{\mathsf{v}}. \tag{30}$$

As shown in Figure 2, in contrast to the evaluation $\bar{\mathbf{u}}_{\text{stream}}|_{\mathbf{p}_i}$ of the raw piecewise-constant field, the evaluation of $\tilde{\mathbf{u}}_{\text{stream}}|_{\mathbf{p}_i}$ at a point vortex has a proper cancellation due to the presence of averaging.

3.1.3 Harmonic Basis. We first build $\boldsymbol{\xi}_\ell$ as the Whitney interpolation [De Goes et al. 2016] of discrete harmonic 1-forms on primal edges. These edge-based discrete harmonic 1-forms are constructed by the tree–cotree algorithm [Crane et al. 2010; Yin et al. 2023]. To construct its dual basis $\boldsymbol{\zeta}_k$, satisfying $\sum_{\mathsf{f}\in\mathsf{F}} \boldsymbol{\zeta}_k(\mathsf{f}) \cdot \boldsymbol{\xi}_\ell(\mathsf{f}) A_{\mathsf{f}} = \delta_{k\ell}$, first define $\tilde{\boldsymbol{\zeta}}_\ell \coloneqq - \star\, \boldsymbol{\xi}_\ell$ as the face-wise rotation of $\boldsymbol{\xi}_\ell$. Compute the $2g$-by-$2g$ incidence matrix $\Lambda_{k\ell} = \sum_{\mathsf{f}\in\mathsf{F}} \tilde{\boldsymbol{\zeta}}_k(\mathsf{f}) \cdot \boldsymbol{\xi}_\ell(\mathsf{f}) A_{\mathsf{f}}$, and let $\boldsymbol{\zeta}_k$ be $\boldsymbol{\zeta}_k \coloneqq \sum_{\ell=1}^{2g} (\Lambda^{-1})^{k\ell} \tilde{\boldsymbol{\zeta}}_\ell$.

3.1.4 Abel–Jacobi Map. The coefficients $\mathbf{a} = (a_1, \dots, a_{2g})$ of the Abel–Jacobi map (21) is defined locally as the piecewise linear function a_ℓ whose gradient equals to $\boldsymbol{\xi}_\ell$. Globally, this local definition leads to either a branch cut (seam) or a multi-valued function. In practice, we keep track of the incremental change of a_ℓ to ensure the value is in the correct branch. Let $\mathbf{p}^{(n)}$ be a point on the mesh at frame n and suppose $\mathbf{p}^{(n+1)}$ is an updated position at the next frame. Then the change $a_\ell|_{\mathbf{p}^{(n)}}^{\mathbf{p}^{(n+1)}} = a_\ell(\mathbf{p}^{(n+1)}) - a_\ell(\mathbf{p}^{(n)})$ is exactly

$$a_\ell|_{\mathbf{p}^{(n)}}^{\mathbf{p}^{(n+1)}} = \int_{\mathbf{p}^{(n)}}^{\mathbf{p}^{(n+1)}} \boldsymbol{\xi}_\ell \tag{31}$$

where $\boldsymbol{\xi}_\ell$ is the piecewise constant 1-form, a Whitney interpolation of a discrete closed 1-form. The integral is independent of the choice of the path on the mesh joining the nearby points $\mathbf{p}^{(n)}$ and $\mathbf{p}^{(n+1)}$.

3.2 The Final ODE

With the spatial discretization (Section 3.1) we turn (25) into the following ODE system.

Algorithm 1 Point vortex solver

Input: Vortices $(\mathbf{p}_i, \kappa_i)_{i=1}^N$; harmonic coefficients $(c_k)_{k=1}^{2g}$; timestep Δt;
for each frame **do**
  $(\mathbf{p}^0, \mathbf{c}^0) \leftarrow (\mathbf{p}, \mathbf{c})$; ▷ Store reference state
  $\mathbf{u}^1 \leftarrow \textsc{Vel}(\mathbf{p}^0; \mathbf{p}^0, \mathbf{c}^0)$; $\mathbf{u}^2 \leftarrow \textsc{Vel}(\textsc{Step}(\mathbf{p}^0, \frac{\Delta t \mathbf{u}^1}{2}); \mathbf{p}^0, \mathbf{c}^0)$;
  $\mathbf{u}^3 \leftarrow \textsc{Vel}(\textsc{Step}(\mathbf{p}^0, \frac{\Delta t \mathbf{u}^2}{2}); \mathbf{p}^0, \mathbf{c}^0)$; $\mathbf{u}^4 \leftarrow \textsc{Vel}(\textsc{Step}(\mathbf{p}^0, \Delta t \mathbf{u}^3); \mathbf{p}^0, \mathbf{c}^0)$;
  $\mathbf{p} \leftarrow \textsc{Step}(\mathbf{p}^0, \frac{\Delta t}{6}(\mathbf{u}^1 + 2\mathbf{u}^2 + 2\mathbf{u}^3 + \mathbf{u}^4))$; $\mathbf{c} \leftarrow \textsc{HarmonicCoeff}(\mathbf{p}; \mathbf{p}^0, c^0)$;
function $\textsc{Step}(\mathbf{p}, \mathbf{d})$ **return** $(\text{Proj}_{\mathsf{M}}(\mathbf{p}_i + \mathbf{d}_i))_{i=1}^N$; ▷ Projected stepping
function $\textsc{Vel}(\mathbf{p}; \mathbf{p}^0, \mathbf{c}^0)$ ▷ Evaluate velocity
  $\bar{\mathbf{u}}_{\text{stream}} \leftarrow \mathcal{J}\,\text{grad}\,\mathbf{L}^{-1}(\sum_i \kappa_i \phi_{\mathsf{v}}(\mathbf{p}_i))_{\mathsf{v}\in\mathsf{V}}$; ▷ (26), (28)
  Compute $\hat{\mathbf{u}}_{\text{stream}}$ and sampler $\tilde{\mathbf{u}}_{\text{stream}}$; ▷ (29), (30)
  $\mathbf{c} \leftarrow \textsc{HarmonicCoeff}(\mathbf{p}; \mathbf{p}^0, \mathbf{c}^0)$;
  return $(\tilde{\mathbf{u}}_{\text{stream}}|_{\mathbf{p}_i} + \sum_{k=1}^{2g} c_k \boldsymbol{\zeta}_k|_{\mathbf{p}_i})_{i=1}^N$; ▷ (33)
function $\textsc{HarmonicCoeff}(\mathbf{p}; \mathbf{p}^0, \mathbf{c}^0)$
  $c_k \leftarrow c_k^0 + \sum_i \kappa_i \int_{\mathbf{p}_i^0}^{\mathbf{p}_i} \boldsymbol{\xi}_k$; **return** $\mathbf{c}$; ▷ (32)

The state variables are the positions $(\mathbf{p}_1(t), \dots, \mathbf{p}_N(t))$ of the point vortices. In contrast to [Yin et al. 2023] where the coefficients c_k for the harmonic components are state variables, in our setting they are implicitly determined by the constant in the last equation of (25). Precisely, given $\mathbf{c}(t_0) = (c_1(t_0), \dots, c_{2g}(t_0))$ at any time t_0, the value of $\mathbf{c}(t)$ is only a function of $(\mathbf{p}_1(t), \dots, \mathbf{p}_N(t))$ by

$$c_k(t) = c_k(t_0) + \textstyle\sum_{i=1}^N \kappa_i \underbrace{a_k|_{\mathbf{p}_i(t_0)}^{\mathbf{p}_i(t)}}_{(31)}, \quad k = 1, \dots, 2g. \tag{32}$$

With this view that $\mathbf{c}$ is a function of $(\mathbf{p}_1, \dots, \mathbf{p}_N)$, we have the final dynamical system for the state variables $(\mathbf{p}_1, \dots, \mathbf{p}_N)$:

$$\boxed{\tfrac{d}{dt}\mathbf{p}_i(t) = \mathbf{u}|_{\mathbf{p}_i(t)}, \quad \mathbf{u} = \underbrace{\tilde{\mathbf{u}}_{\text{stream}}}_{\text{Section 3.1.2}} + \textstyle\sum_{k=1}^{2g} c_k \boldsymbol{\zeta}_k.} \tag{33}$$

In practice, we employ a projected 4th order Runge–Kutta (RK4) for solving this ODE. That is, each of the four intermediate forward-Euler steps in RK4 is composed with an orthogonal projection back to the surface. After each frame is solved, we update t_0 in (32) as the current frame, so that the variables $\mathbf{p}_i$ that are evaluated during the next RK4 step are always close to $\mathbf{p}_i(t_0)$.

With the harmonic bases $(\boldsymbol{\xi}_\ell, \boldsymbol{\zeta}_\ell)_{\ell=1}^{2g}$ (Section 3.1.3) and Laplacian $\mathbf{L}$ precomputed, the algorithm is summarized in Algorithm 1.

3.2.1 Timestep. For stable RK4 integration, the timestep Δt must resolve the timescale of the ODE system. Since the velocity $\mathbf{u}|_{\mathbf{p}_i}$ scales as κ/d, where κ is the vortex strength and d the inter-vortex distance, dimensional analysis gives $\Delta t \sim d^2/\kappa$, *i.e.*, inversely with the vorticity-sampling density.

3.2.2 Discussion. If the streamfunction velocity $\tilde{\mathbf{u}}_{\text{stream}}$ in (33) is replaced by the piecewise-constant field $\bar{\mathbf{u}}_{\text{stream}}$ from (28), then the resulting ODE becomes a Hamiltonian system, with the Hamiltonian given by the discrete kinetic energy $H(\mathbf{p}_1, \dots, \mathbf{p}_N) = \frac{1}{2}\sum_{\mathsf{f}\in\mathsf{F}} |\mathbf{u}|^2$, $\mathbf{u} = \bar{\mathbf{u}}_{\text{stream}} + \sum_{k=1}^{2g} c_k \boldsymbol{\zeta}_k$ for the classical symplectic structure [Marsden and Weinstein 1983; Boatto and Koiller 2008] for point vortices. In fact, since the discrete vorticity (27) is obtained from the point vortices via the adjoint $\mathcal{I}^*$ of $\mathcal{I}$, this Hamiltonian system is equivalent to the *$\mathcal{I}$-discrete Euler equation* introduced in [Nabizadeh et al. 2024]. More specifically, the auxiliary symplectic space parameterizing the

Table 1. Parameters for each experiment.

	vortex count	vortex strength (m^2/s)	Δt (s)
Fig. 3	1	1	0.01
Fig. 4	2	1	0.01
Fig. 5, 6	2	1	0.1
Fig. 7	2	1	0.5
Fig. 8	1 (2)	1	0.01
Fig. 9	2	1	0.05
Fig. 10 top	10^5	2×10^{-5}	10^{-3}
Fig. 10 mid.	10^5	2×10^{-5}	10^{-4}
Fig. 10 bot.	10^5	2×10^{-5}	10^{-4}

coadjoint orbit is the symplectic manifold of point vortices, and $\mathcal{I}^*$ is the momentum map on this space. Using point vortices as the auxiliary symplectic space was previously explored on Cartesian grids with B-spline finite elements in [Nabizadeh 2025].

Although replacing $\tilde{\mathbf{u}}_{\text{stream}}$ with $\bar{\mathbf{u}}_{\text{stream}}$ in (33) preserves the Hamiltonian structure preservation, we observe that, for piecewise-linear and piecewise-quadratic elements, the resulting vortex dynamics deviates noticeably from the continuous dynamics, as shown in Figure 2. One possible explanation is that the kinetic energy of a point vortex diverges in the continuous limit, leading to a discrepancy when the kinetic energy is directly restricted to the discrete subspace and used as the Hamiltonian. In the smooth theory, the appropriate normalized Hamiltonian for point vortices is the Kirchhoff–Routh function, which involves the Robin function [Boatto and Koiller 2008; Grotta-Ragazzo et al. 2024]. We therefore expect that the behavior of piecewise-linear $\mathcal{I}$-discrete Euler flow on coadjoint orbits of point vortices would more faithfully reproduce the continuous dynamics if the Hamiltonian were replaced by the Kirchhoff–Routh function.

4 Results

Our implementation uses a combination of Python and SideFX Houdini. The main computational components, including the Poisson solve, RK4 time integration of the ODE states, barycentric velocity smoothing, and harmonic basis computation, were performed in Python on the CPU. All experiments were run on an Apple MacBook Pro with an Apple M3 Pro chip based on ARM architecture, with an 11-core CPU and 18 GB of unified memory. For a typical mesh, such as the torus example shown in Figure 7 with approximately 6K triangles, the simulation runs at about 1.4 seconds per frame. The parameters for each experiment are listed in Table 1.

4.0.1 Analytical solution on an annulus. We validate our solver against the analytical solution for point-vortex motion in an annulus, namely the planar region bounded by two concentric circles of radii r_a and r_b. The vortex dynamics on this domain can be interpreted as dynamics on the torus obtained by doubling the annulus; see App. A. The analytical solution for the vortex dynamics is derived in App. B and [Crowdy and Marshall 2005]. In this configuration, a positive point vortex is expected to travel counterclockwise along a circle of constant radius with a specific speed. The harmonic component is conserved throughout the motion, and we initialize it to zero. This therefore provides a benchmark for comparing the numerical streamfunction velocity $\tilde{\mathbf{u}}_{\text{stream}}$ against the analytical velocity.

Figure 3 shows that our method produces vortex trajectories that remain on the expected circular orbits. In addition, we evaluate $\tilde{\mathbf{u}}_{\text{stream}}|_{\mathbf{p}}$ on the vortex positions $\mathbf{p}$ for various $r_A < |\mathbf{p}| < r_B$. The plots demonstrate close agreement between the numerical and analytical velocities.

4.0.2 Vortex Pair Passing between Obstacles. Yin et al. [2023] introduced a benchmark involving a vortex pair traveling through the narrow region between two obstacles in a planar domain. The physically correct behavior is for the vortex pair to pass through this region. Without accounting for the interaction between the harmonic components and the vorticity, the vortices are deflected away from the passage. Figure 9 shows that our method successfully reproduces this benchmark.

4.0.3 Dipoles on Curved Surfaces. A close pair of vortices (a dipole) move along geodesics on a surface. This is known as *Kimura's conjecture*, proven in [Boatto and Koiller 2008] and [Gustafsson 2022]. Numerical demonstrations of this phenomenon on topological spheres were given by [Padilla 2018].

We show Kimura's phenomenon for both a sphere and a torus. Figure 4 demonstrates that a vortex pair in our method follows a great circle. Figure 5 shows a dipole motion on a torus, which also traces out a geodesic.

Note that this dipole simulation is difficult to reproduce in the previous Eulerian functional fluid methods [Azencot et al. 2014; Yin et al. 2023] as shown in Figure 6, due to excessive dispersion. Our point vortex simulation is able to preserve the long-term vortex details even on a relatively low resolution mesh.

4.0.4 Vortex–Harmonic Interaction on a Torus. The examples of Section 4.0.3 exhibit only negligible interaction between the vortices and the harmonic component, since nearby vortices of opposite signs yield $\mathrm{AJ}(D) \approx 0$ throughout the evolution. To demonstrate a nontrivial interaction between the vortices and harmonic components, in Figure 7 we place a positive vortex on the outer region of the torus and a negative vortex near the inner neck. The harmonic component is initialized as a poloidal flow. This configuration induces substantial motion of $\mathrm{AJ}(D)$ in the Jacobi variety. Our simulations show that updating the harmonic components with the Abel–Jacobi coordinates leads to qualitatively different behavior compared to the case in which the harmonic dynamics are neglected. In fact, as the vortices rotate away from the equator, a toroidal flow is expected to emerge to conserve the vertical component of the angular momentum. This phenomenon is captured in our method.

4.0.5 Vortex Sheets on Curved Surfaces. Figure 10 showcases vortex sheet simulations on the sphere, the genus-1 Bob model, and a genus-2 Lawson surface. The vorticity distribution is sampled by N (100,000) point vortices using an off-the-shelf scattering tool, with a constant $1/N$ weight per particle. Our point-vortex solver is capable of reproducing energetic Kelvin–Helmholtz instability patterns on geometrically and topologically complex surfaces.

4.0.6 Non-Orientable Surfaces. Figure 8 shows a point vortex simulation on a Möbius strip, which is non-orientable. Our simulation runs on its oriented double cover, where each point vortex is accompanied by a duplicate of opposite sign. A fluid system with this parity symmetry is equivalent to a fluid simulation on the underlying non-orientable surface.

5 Summary

We presented a point-vortex solver for curved surfaces with arbitrary topology. Our main contribution is identifying a fundamental connection between vortex dynamics and the theory of divisors on Riemann surfaces. In particular, we show that the difference between the harmonic component and the Abel–Jacobi coordinate of the vortex configuration is a conserved quantity. To the best of our knowledge, this invariant has not been stated in the literature.

By exploiting this conservation law, the dynamics of the harmonic component can be absorbed into the vortex evolution equation, which can then be discretized using recent vortex particle-on-mesh methods. Beyond its computational simplicity, this perspective reveals a rich interplay between complex-analytic geometry processing and fluid dynamics on multiply connected surfaces.

Limitations. Our point-vortex solver is limited to inviscid fluids. From a numerical analysis perspective, the velocity interpolation in Section 3.1.2 s not yet accompanied by a convergence proof. In terms of structure preservation, while our method exactly conserves circulation (as quantified by the Casimir invariants, including the individual vortex strengths and the conserved quantity involving the Abel–Jacobi coordinate), it remains unclear whether energy conservation can be meaningfully defined or measured. In the point-vortex limit, the classical kinetic energy is infinite; after discretization, this energy can be rather arbitrary and diverges under mesh refinement. The appropriate renormalized energy is the Kirchhoff–Routh function, whose construction on discrete surfaces is, to our knowledge, not yet known in the literature. Addressing these questions constitutes important directions for future work.

Acknowledgments

This work is supported by the NSF CAREER Award 2239062. Additional support is provided by SideFX.

References

Hassan Aref. 2007. Point vortex dynamics: a classical mathematics playground. *Journal of mathematical Physics* 48, 6 (2007).

Omri Azencot, Steffen Weißmann, Maks Ovsjanikov, Max Wardetzky, and Mirela Ben-Chen. 2014. Functional fluids on surfaces. In *Computer Graphics Forum*, Vol. 33. Wiley Online Library, 237–246.

George Keith Batchelor. 1967. *An introduction to fluid dynamics*. Cambridge university press.

Stefanella Boatto and Jair Koiller. 2008. Vortices on closed surfaces. *arXiv preprint arXiv:0802.4313* (2008).

VA Bogomolov. 1977. Dynamics of vorticity at a sphere. *Fluid Dynamics* 12, 6 (1977), 863–870.

Keenan Crane, Fernando De Goes, Mathieu Desbrun, and Peter Schröder. 2013. Digital geometry processing with discrete exterior calculus. In *ACM SIGGRAPH 2013 Courses*. ACM, 1–126.

Keenan Crane, Mathieu Desbrun, and Peter Schröder. 2010. Trivial connections on discrete surfaces. In *Computer Graphics Forum*, Vol. 29. Wiley Online Library, 1525–1533.

DG Crowdy, EH Kropf, CC Green, and MMS3564667 Nasser. 2016. The Schottky–Klein prime function: a theoretical and computational tool for applications. *IMA journal of applied mathematics* 81, 3 (2016), 589–628.

Darren Crowdy and Jonathan Marshall. 2005. Analytical formulae for the Kirchhoff–Routh path function in multiply connected domains. *Proceedings of the Royal Society A: Mathematical, Physical and Engineering Sciences* 461, 2060 (2005), 2477–2501.

Qiaodong Cui, Timothy Langlois, Pradeep Sen, and Theodore Kim. 2021. Spiral-spectral fluid simulation. *ACM Transactions on Graphics (TOG)* 40, 6 (2021), 202:1–202:16.

Fernando De Goes, Mathieu Desbrun, and Yiying Tong. 2016. Vector field processing on triangle meshes. In *ACM SIGGRAPH 2016 Courses*. ACM, 1–49.

Sharif Elcott, Yiying Tong, Eva Kanso, Peter Schröder, and Mathieu Desbrun. 2007. Stable, circulation-preserving, simplicial fluids. *ACM Transactions on Graphics (TOG)* 26 (2007). Issue 1.

Otto Forster. 2012. *Lectures on Riemann surfaces*. Springer Science & Business Media.

Clodoaldo Grotta-Ragazzo, Björn Gustafsson, and Jair Koiller. 2024. On the interplay between vortices and harmonic flows: Hodge decomposition of Euler's equations in 2D. *Regular and Chaotic Dynamics* 29, 2 (2024), 241–303.

Xianfeng David Gu and Shing-Tung Yau. 2008. *Computational Conformal Geometry*. International Press.

Björn Gustafsson. 2022. Vortex pairs and dipoles on closed surfaces. *Journal of Nonlinear Science* 32, 5 (2022), 62.

Anil Nirmal Hirani. 2003. *Discrete exterior calculus*. California Institute of Technology.

Nikolai Joukowsky. 1910. Über die konturen der Tragflächen der Drachenflieger. *Zeitschrift für Flugtechnik und Motorluftschiffahrt* 1, 22 (1910), 281–285.

John M Lee. 2024. *Introduction to complex manifolds*. Vol. 244. American Mathematical Society Providence, RI.

Jerrold Marsden and Alan Weinstein. 1983. Coadjoint orbits, vortices, and Clebsch variables for incompressible fluids. *Physica D: Nonlinear Phenomena* 7, 1-3 (1983), 305–323.

Mohammad Nabizadeh. 2025. *Fluid Dynamics: From Geometric Formulations to Structure-Preserving Simulations*. Ph. D. Dissertation. University of California San Diego. https://www.proquest.com/dissertations-theses/fluid-dynamics-geometric-formulations-structure/docview/3226972823/se-2 Copyright - Database copyright ProQuest LLC; ProQuest does not claim copyright in the individual underlying works; Last updated - 2025-07-23.

Mohammad Sina Nabizadeh, Ritoban Roy-Chowdhury, Hang Yin, Ravi Ramamoorthi, and Albert Chern. 2024. Fluid Implicit Particles on Coadjoint Orbits. *TOG* 43, 6 (2024), 270:1–270:38.

Ingo Nitschke, Sebastian Reuther, and Axel Voigt. 2017. Discrete exterior calculus (DEC) for the surface Navier-Stokes equation. In *Transport processes at fluidic interfaces*. Springer, 177–197.

Ingo Nitschke, Sebastian Reuther, and Axel Voigt. 2021. Vorticity-stream function approaches are inappropriate to solve the surface Navier-Stokes equation on a torus. *PAMM* 20, 1 (2021), e202000006.

Marcel Padilla. 2018. Point Vortex Dynamics on Closed Surfaces. *M.S. Thesis* (05 2018).

Philip G Saffman. 1992. Vortex dynamics. In *Theoretical Approaches to Turbulence*. Springer, 263–277.

Andrew Selle, Nick Rasmussen, and Ronald Fedkiw. 2005. A vortex particle method for smoke, water and explosions. In *ACM SIGGRAPH 2005 Papers*. Association for Computing Machinery, New York, NY, USA, 910–914.

Lin Shi and Yizhou Yu. 2004. Inviscid and incompressible fluid simulation on triangle meshes. *Computer Animation and Virtual Worlds* 15, 3-4 (2004), 173–181.

Jos Stam. 2003. Flows on surfaces of arbitrary topology. *ACM Transactions On Graphics (TOG)* 22, 3 (2003), 724–731.

Ningxiao Tao, Liangwang Ruan, Yitong Deng, Bo Zhu, Bin Wang, and Baoquan Chen. 2024. A Vortex Particle-on-Mesh Method for Soap Film Simulation. *TOG* 43, 4 (2024), 53:14–53:14.

Joris Vankerschaver and Melvin Leok. 2014. A novel formulation of point vortex dynamics on the sphere: geometrical and numerical aspects. *Journal of Nonlinear Science* 24, 1 (2014), 1–37.

Stephanie Wang, Mohammad Sina Nabizadeh, and Albert Chern. 2023. Exterior Calculus in Graphics: Course Notes for a SIGGRAPH 2023 Course. In *ACM SIGGRAPH 2023 Courses* (Los Angeles, California) *(SIGGRAPH '23)*. Association for Computing Machinery, New York, NY, USA, Article 8, 126 pages. doi:10.1145/3587423.3595525

Larry Yaeger, Craig Upson, and Robert Myers. 1986. Combining physical and visual simulation—creation of the planet jupiter for the film "2010". *Acm Siggraph Computer Graphics* 20, 4 (1986), 85–93.

Hang Yin, Mohammad Sina Nabizadeh, Baichuan Wu, Stephanie Wang, and Albert Chern. 2023. Fluid Cohomology. *TOG* 42, 4 (2023), 126:1–126:25. doi:10.1145/3592402

Cuncheng Zhu, Hang Yin, and Albert Chern. 2025. Viscous Vortex Dynamics on Surfaces. *TOG* 44, 6 (2025), 178:1–178:21.

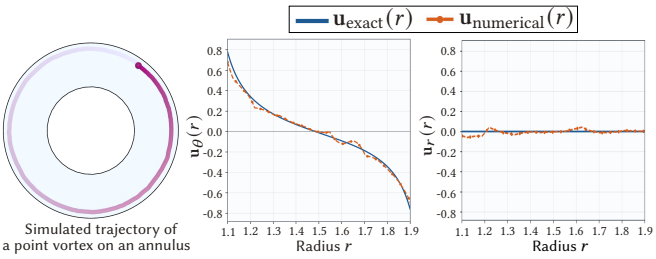


Fig. 3. A point vortex in an annulus bounded by concentric circles of radius $r_a = 1$ and $r_b = 2$. The plots compare the numerical and analytic values of the streamfunction velocity $\mathbf{u}_{\text{stream}}|_{\mathbf{p}} = (u_r, u_\theta)$ at the point vortex, in the tangential (u_θ) and radial (u_r) components, for various radial location $r_a < |\mathbf{p}| < r_b$ of the vortex. The averaged edge length of the triangulated annulus is about 0.1.

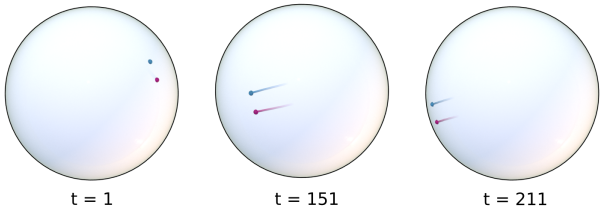


Fig. 4. Vortex pair on a sphere, approximately following a great arc.

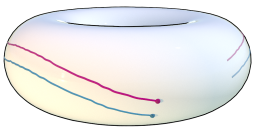


Fig. 5. Vortex pair on a torus, approximately following a geodesic.

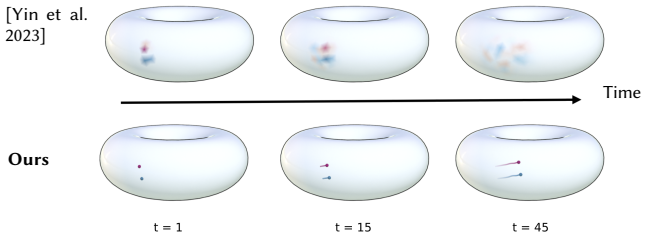


Fig. 6. Our point vortex simulation is able to preserve concentrated vorticity configuration significantly better than Eulerian methods.

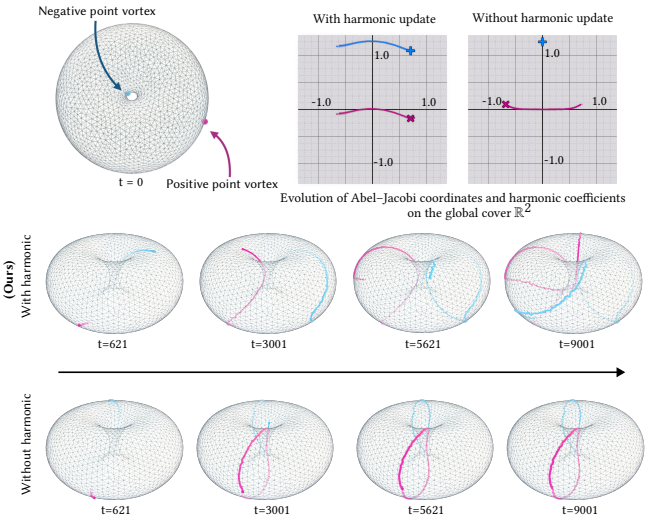


Fig. 7. Vortex dynamics on a torus with initial condition shown in top-left. Our simulations show that updating the harmonic components with the Abel–Jacobi coordinates leads to qualitatively different behavior compared to the case in which the harmonic dynamics are neglected. Top-right: Time evolution of the Abel–Jacobi image of the vortex positions (red) and harmonic coefficients (blue) on the $\mathbb{R}^{2g}$ universal cover of the Jacobi variety.

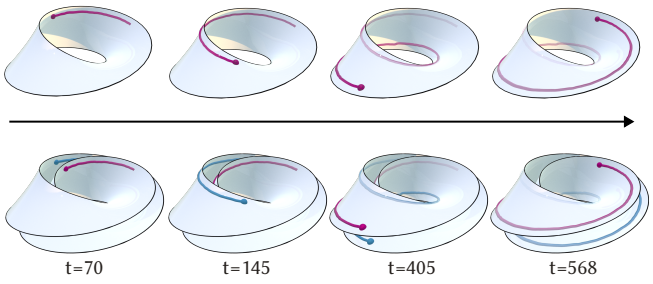


Fig. 8. Point vortex dynamics on a non-orientable Möbius strip (top row). The simulation is performed on the orientable double cover of the strip, where each vortex is paired with a duplicate of opposite sign (bottom row).

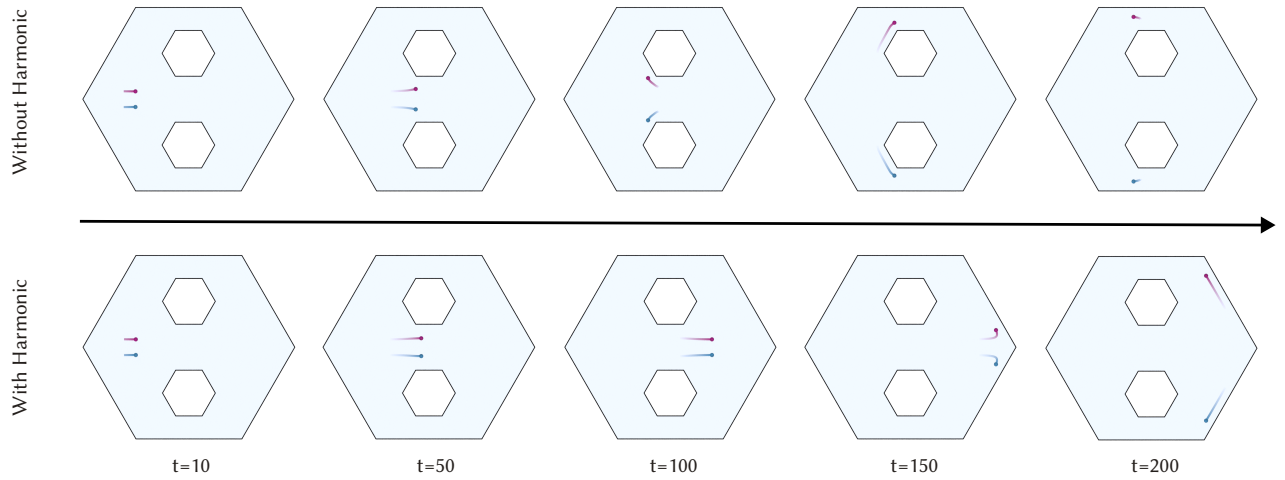


Fig. 9. Vortex pair passing between obstacles, a benchmark introduced in [Yin et al. 2023]. Without updating the harmonic coefficients, the vortices are deflected away from the region between the obstacles (top). By incorporating the harmonic component (bottom) through the Abel–Jacobi map, the vortex pair passes through the gap, consistent with the results reported in [Yin et al. 2023].

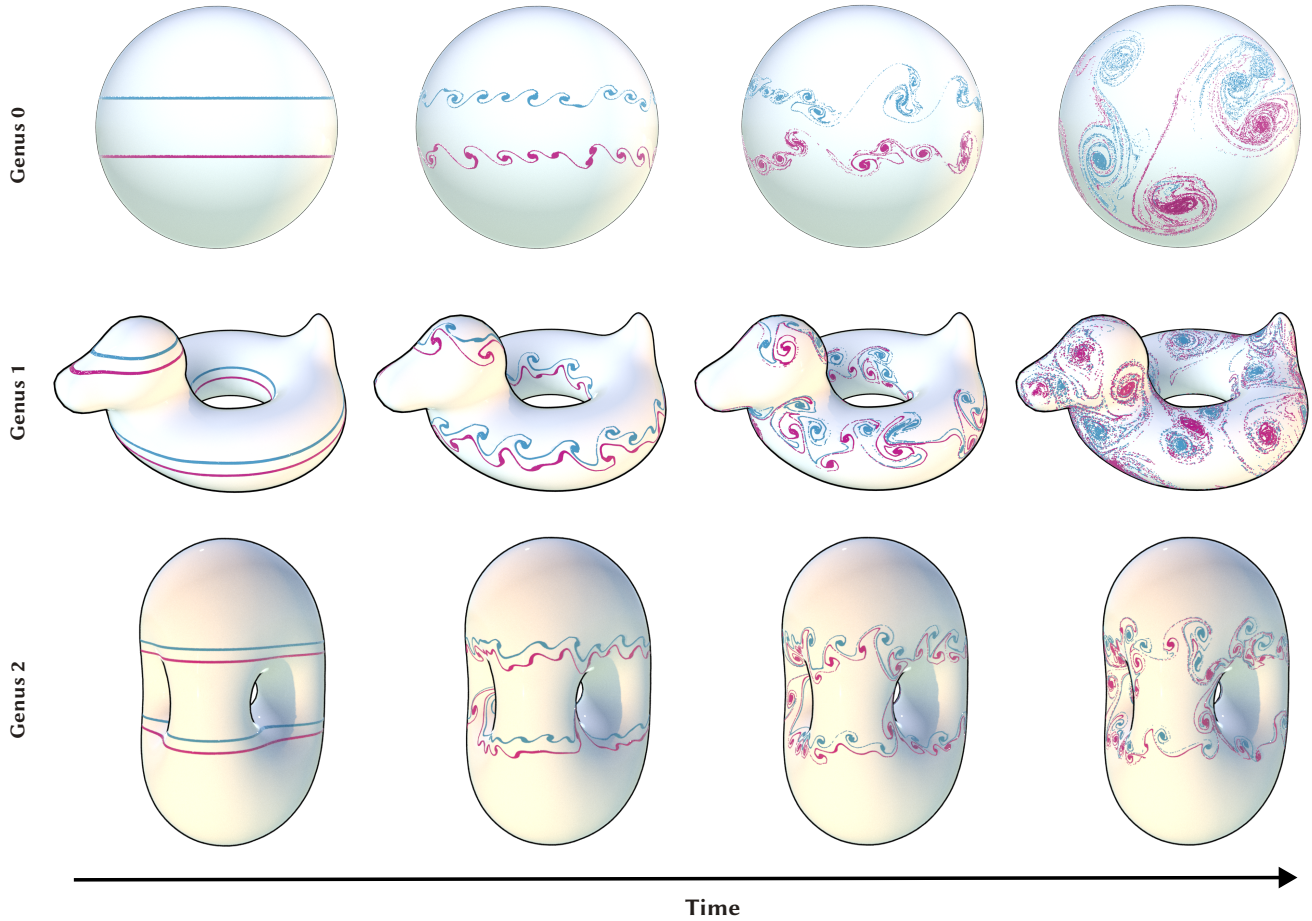


Fig. 10. Vortex-sheet simulations on curved surfaces with varying genus.